QNDE2022- ####

CRAWLER-BASED AUTOMATED NON-CONTACT ULTRASONIC INSPECTION OF LARGE STRUCTURAL ASSETS

Ross McMillan[1], Morteza Tabatabaeipour[1], Konstantinos Tzaferis[1], William Jackson[1], Rachel S. Edwards[2], Oksana Trushkevych[2], Charles Macleod[1], Gordon Dobie[1], Anthony Gachagan[1]

[1] Centre for Ultrasonic Engineering, Department of Electronic and Electrical Engineering, University of Strathclyde, Glasgow G11XW, UK
[2] Department of Physics, University of Warwick, Coventry CV4 7AL, UK
r.mcmillan@strath.ac.uk

ABSTRACT

This paper presents an update on the progress of developing a crawler-based automated non-contact ultrasonic inspection system for the evaluation of large structural assets. The system presented is a significant improvement on current robotic NDT crawlers and aims to greatly reduce the time of inspection by creating an internal feature map of the subject in a Simultaneous Localisation And Mapping (SLAM) style method instead of using a lawnmower scanning style where all areas are scanned regardless if they contain features or are featureless. This map will be generated through rapid automated path planning and scanning and will show the location of potential areas of interest, where then, the appropriate method of inspection can be used for a high detailed evaluation. Current and ongoing work presented is as follows; the use of guided waves as the sensory input of an occupancy grid map; evaluating guided wave modes to find the mode most appropriate for this system; minimum thickness estimation using machine learning; improving the transducer setup using a unidirectional transmitter.

Keywords: Guided Waves, EMATs, Shear Horizontal, Mobile Robotic Crawlers, Occupancy Grid Mapping.

1. INTRODUCTION

There is an industrial drive and statutory need to monitor the integrity and condition of industrial assets such as pipelines, tanks and vessels, in order to ensure optimum operational uptime, prevent failures and costly forced outages [1]. Non-Destructive Evaluation (NDE) is an effective method to assess the structural integrity of these assets and identify any degradation, deviations or defects. Suitable NDE techniques require precise detection, location and measurement of structural parameters such as corrosion and thickness, in a nonintrusive manner, with the results utilised to make informed decisions on future operational activities and maintenance. Automation of

NDE offers the potential to address some of the limitations of traditional manual NDE, which suffers from slow inspections, increased costs to ensure inspection safety, inconsistent measurements through poor human repeatability and an inability to access certain hazardous locations [2]. Research in automated and robotically deployed NDE seeks to address these limitations and obtain a decrease in inspection time and cost while improving inspection accuracy and safety [3]. The current state-of-the-art automated NDE seeks to combine inspection modalities such as ultrasonic [3], [4], vision [5], optical [6] and electromagnetic [7], [8], sensing techniques with robotic platforms and data analysis and interpretation software, to enable fast and intelligent inspection [9]. Ultrasonics is an inspection technique that utilises acoustic waves of frequency 20 kHz or greater to inspect industrial assets through wave propagation and analysis of parameters such as time-of-flight and amplitude [10]. Ultrasonics is a safe and sensitive inspection modality capable of measuring asset parameters such as wall thickness, corrosion loss and weld cracking [11]. Current state-of-the-art industrial ultrasonic NDE implemented on robots [3], [12], typically measures component thickness and corrosion through the use of normal incidence bulk wave inspection, directed perpendicularly into the subject surface [13]. These waves are typically generated using single-element or phased array bulk wave transducers, which require contact with the sample. Although quicker and cheaper than manual NDE, such approaches are still time-consuming as the probes are required to be scanned across the full area to achieve the desired coverage [4]. Furthermore, such systems typically estimate their position using wheel encoders, which drift over time, especially when not travelling in a straight line [14]. There are limited localisation systems available that provide the appropriate level of global accuracy (~10mm), and those that do exist, such as Laser Trackers [15], are prohibitively expensive (2-3x the cost of inspection robots). Combining

medium-range inspection techniques with on-board localisation, both using ultrasonic guided waves, can improve automated inspection using robotics in these two key areas. This paper describes the current state of the art in the development of this system.

The first section will give a project overview describing the system at a high level and the goals of the project. The second section will be a summary of the first work published, presenting the proof of concept of the system. The third section is a summary of the work on selecting the most appropriate guided wave mode for this system.

2. PROJECT OVERVIEW

The aim of this project is to develop a robotic crawler system that can automatically and quickly create a structural map of a subject. This map will include structural defects, welded regions, geometrical features etc. These internal and surface features will be detected using guided waves generated within the subject of interest. The robotic crawler will use guided waves to range and estimate the position of the internal features relative to itself, using this information it will continue to range and map by following features it has detected and looking for unknown areas to build up a map in a SLAM style method, [16], [17]. The crawler will move around the surface of the subject being guided by the internal features it detects. This method is efficient as the system automatically generates the robot's path based on features that have been detected and by looking to move to unexplored areas of the subject, which greatly decreases inspection time compared to methods that use lawnmower scanning style methods as there is little overlapping on previously explored areas.

The use of guided waves compared to bulk ultrasonic methods greatly decreases inspection time too, this is due to the significantly longer propagation distance of guided waves, which allows a significantly larger portion of the subject to be scanned in a shorter time. Further to this another benefit to using guided waves in mapping and ranging scenarios is the longer propagation distance, which makes it possible to scan inaccessible areas where the transducer cannot make direct contact with.

FIGURE 1: CAD MOCKUP OF FINAL SYSTEM OPERATING ON A PRESSURE VESSEL.

The combination of an automated path planning and mapping algorithm with guided waves shows significant benefits over current industry standard robotic NDT inspection systems, an image of this concept is shown in Fig. 1. It must be stated however that guided waves are not being used as the primary inspection method for evaluating defects and that the goal of this system is to quickly identify the areas of interest and their location, so that the appropriate method of inspection can then be used to fully define the problem area.

3. GUIDED WAVE OCCUPANCY GRID MAPPING

The first step in this project was to show that guided waves could be used for ranging and mapping, [18] was produced to show proof of concept of the guided wave occupancy grid mapping system (GW-OGM).

In this work SH0 was used as the sensory input for a transmitter model that operated within an Occupancy Grid Map (OGM). Occupancy grid mapping is a probabilistic mapping algorithm in the field of mobile robotics which addresses the problem of generating maps from noisy and uncertain sensor measurement data, in this case guided waves, with the assumption that the robot pose is known [19].

Conceptually the OGM simply partitions a 2D environment into cells, with each being the probability of three states, including free, occupied, and unknown, the sensory input for the OGM in this work is guided wave ranging measurements. Values close to 1 (black) represent a high probability that the cell contains an obstacle (in this work, obstacle refers to the geometrical features of a component such as edges/welded regions). Values close to 0 (white) represent a high probability that the cell is obstacle-free. As the robot drives around learning the environment, the unknown cells are filled in. Bayesian probability is then used to update probabilities when the new measurements are taken for any given cell. Information about which areas are unknown is also important, e.g., for autonomous exploration of an environment. In OGM, sensor readings are transformed into probabilities and then combined using Bayes' rule for data fusion [43]. A standard occupancy grid map calculates the posterior over the map $p(m_i|z_{1:t}, x_{1:t})$ given a set of measured data up to time $(z_{1:t})$, and the robot poses $(x_{1:t})$, which are assumed to be known, and part of the measurement here, the full expansion of this can be found in [18].

The OGM was then simulated with a bidirectional Electromagnetic Acoustic Transducer (EMAT) transmitter and two EMAT receivers, a sensor model was created for this so that it was represented in the OGM algorithm. Two receivers were used, as a bidirectional transmitter produces waves propagating forwards and backwards, so two receivers are required in order to identify the direction of propagation. Incorporating the sensor model into the OGM, the model was simulated, in this simulation however the robot's path was predefined as at this point of the work, a proof concept was needed to show that guided waves could be used to map, where automated path planning will be carried out in future work but is not necessary for proof of concept.
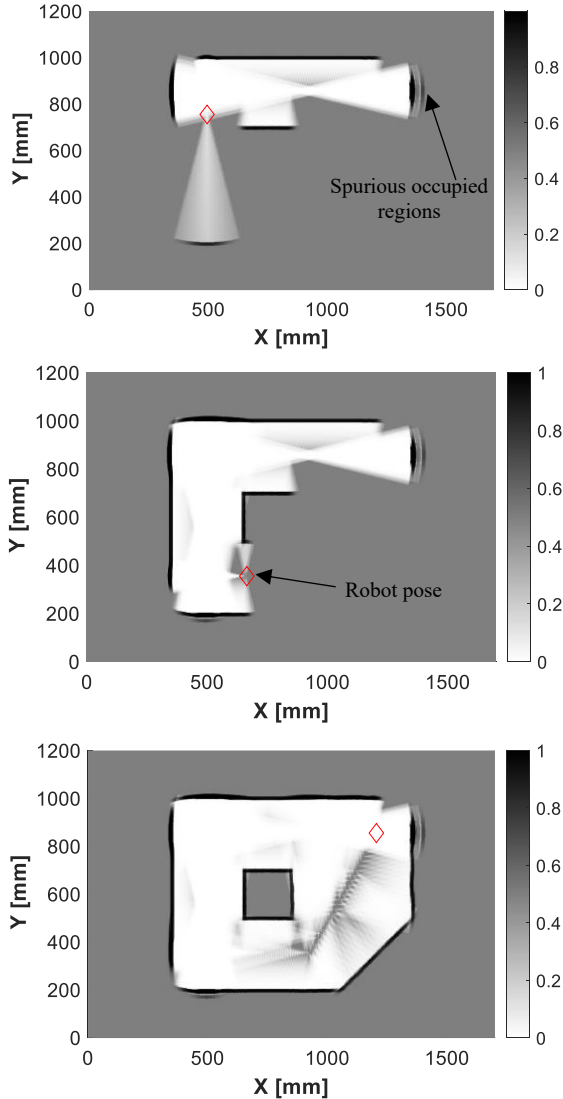
FIGURE 2: IMAGES OF THE OCCUPANCY GRID MAP WITH THE SIMULATED SENSOR MODEL; THE RED DIAMOND REPRESENTS THE ROBOTIC CRAWLER.

Fig. 2 shows the simulation of the model. The red diamond represents the robot crawler and the position of the transducer setup, this diamond moves across the surface of the sample generating guided waves in the plate. As the robot moves and guided waves are received cells turn from grey, unknown, to white or black, which is free or occupied, respectively. As the robot continues to move the edges of the plates become clear and the full shape can be seen. This simulation proved that guided waves could be used as the sensory input for mapping, the next step for the mapping algorithm is to fully automate this system to incorporate automated path planning for the robotic crawler.

4. CHOICE OF GUIDED WAVE MODE FOR GW-OGM

For the work in [18] SH0 was used as the guided wave mode for sensory input as it is non-dispersive, however this choice had to be evaluated in more detail as looking at the structures that

this system is likely to inspect, welds are commonplace so will be a suitable feature to localise and act as anchors for the maps. As a result, the choice of guided wave mode was evaluated by testing five wave modes (A0, S0, S1, SH0, SH1) and their reflectivity from welds [20].

It was thought that the energy density distribution of a wave mode would be a key indicator of its reflectivity from welds. The energy density distribution of a mode is the portion of the waves energy in a given point in the plates thickness [21]. Considering the geometry of a weld on plate, the presence of a weld head causes an increase from nominal plate thickness, the wave mode which is best suited to ranging will react to this change in thickness by strongly reflecting from it. This requires the mode to be sensitive to upper and lower boundary changes. The energy density distribution of a wave mode can then be used to identify the areas of a plate thickness which carry the largest portions of a wave's energy, as this is not always constant across the thickness. The theoretical energy distributions of the five modes tested in 10 mm steel plate are shown in Fig. 3. It can be seen that SH1 has the highest overall energy and a significant portion of its energy favours the top and bottom boundaries of the plate, as such it was thought that SH1 would likely have the highest reflectivity in testing.
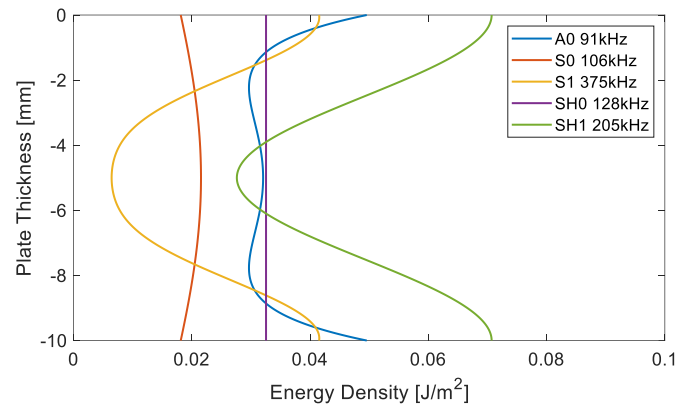

FIGURE 3: ENERGY DENSITY DISTRIBUTIONS ACROSS 10MM PLATE FOR A0, S0, S1, SH0 AND SH1 GENERATED USING DISPERSION CALCULATOR.

The modes were tested by using a transmitter EMAT to propagate a wave towards a receiver EMAT, the wave moves past the receiver towards a weld, the wave reflects from the weld and returns to the receiver, this setup can be seen in Fig. 4. The reflected signal was then divided by the first received wave to gain a reflection coefficient, this allowed easy comparison of each of the modes reflectivity through a single value.
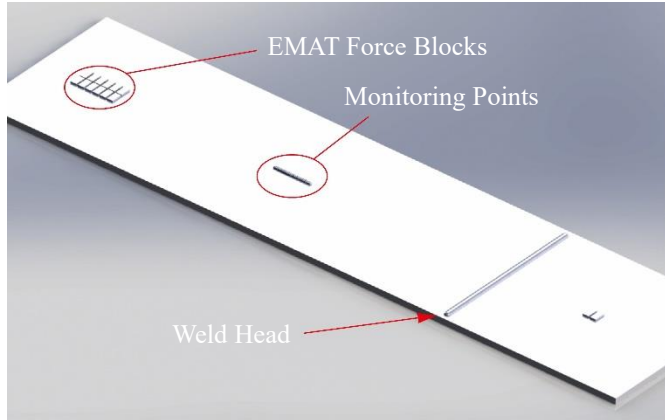
FIGURE 4: REFLECTION COEFFICIENT MEASUREMENT SETUP SHOWN IN SIMULATION. IN THE EXPERIMENT, THE 64 MONITORING POINTS WERE REPLICATED BY MOVING THE RECEIVER EMAT IN 64 1MM STEPS.

All five modes were tested in simulation in four different 10mm steel plates, each of the four plates had a different weld head size so that wave mode stability could be measured, this was needed as a wave mode whose reflectivity increased as the weld head increased in a stable fashion would be better suited to ranging and mapping, than a mode which had reflectivity that varied greatly with small changes in weld head size.

The results of the simulation are shown in Fig. 5, it can be seen that the reflectivity of the modes tested corresponded with the energy density distributions shown in Fig. 3. The modes with higher reflectivity had energy density distributions that favoured the plate boundaries. SH0 and SH1 were then tested in an experiment using an identical setup to the simulation, similar results were found; however, reflection coefficients were reduced in value by approximately 0.1-0.2.
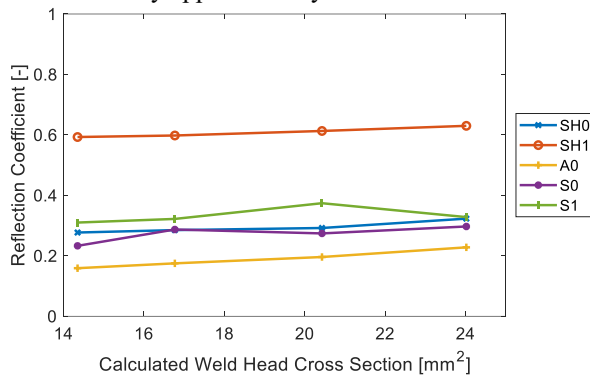

FIGURE 5: REFLECTION COEFFICIENT VALUES FOR EACH MODE IN EACH OF THE FOUR SAMPLES. IT CAN BE SEEN SH1 IS SIGNIFICANTLY MORE REFLECTIVE THAN THE OTHER MODES TESTED.

From this study it was found that SH1 would be the best-suited wave mode to use for ranging and mapping, considering the structures that would likely be under inspection.

5. MINIMUM REMAINING WALL THICKNESS ESTIMATION USING GUIDED WAVES

To increase the amount of information in the map produced by the system thickness estimation of the minimum remaining wall thickness using Gaussian process regression machine learning [22]. This increases the amount of information on the map, which is better for the inspector when choosing the high detail method of inspection to evaluate an area of interest, and it also increases the certainty of the type of feature under inspection. The machine learning model was designed to be able to predict the depth and width of defects using the instantaneous phase of the received signals, Fig. 6.
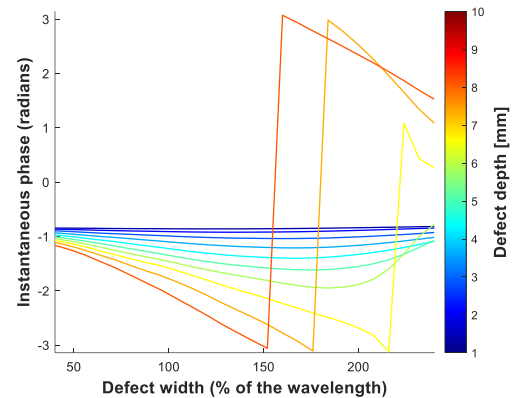

FIGURE 6: A TYPICAL PATTERN OF INSTANTANEOUS PHASE VARIATION OF SH0 WAVE MODE AS A FUNCTION OF WIDTH FROM SIMULATION DATA FOR A CIRCULAR DEFECT.

OnScale (OnScale, US-CA) was used to create a dataset which featured a number of defects in plates for the machine learning model. From this model experimental tests were carried out where a transmitter and receiver EMAT setup was moved across an aluminium plate, where waves were sent from transmitter to receiver as the setup is moved perpendicular to the direction of wave propagation, Fig. 7. This plate has three flat bottom holes of varying width and depth, the goal of this experiment was to use the machine learning model and instantaneous phase method to determine the size of the defects.
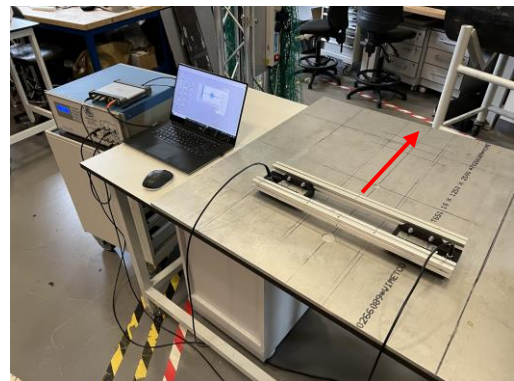

FIGURE 7: EXPERIMENTAL SETUP TO MEASURE THE THREE FLAT BOTTOM HOLES; THE ARROW INDICATES THE DIRECTION OF TRANSDUCER MOVEMENT.

The machine learning model was able to accurately estimate the depth and width of two of the defects and the width of the third defect, this can be seen in Fig. 8. The third defects depth is 90% of the plates thickness and has a width that is smaller than the wavelength of the guided wave, this is a difficult defect to accurately measure, however future work is looking to solve this as well as explore the estimation of varying defect shapes which will better represent real world defects.
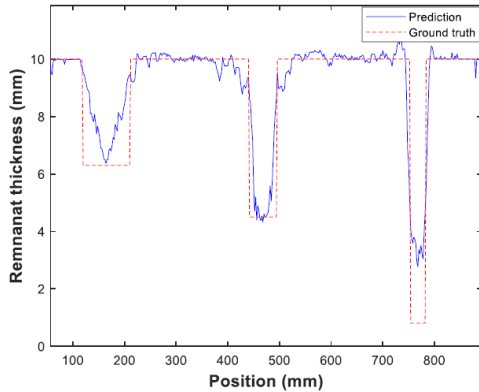

FIGURE 8: ESTIMATION OF REAL DATA SET CONTAINING THREE FBH DEFECTS USING THE GPR MODEL, SHOWING A GOOD ESTIMATION OF WIDE DEFECTS (DEFECT WIDTH TO WAVELENGTH RATIO OF ≥100%).

6. UNI-DIRECTIONAL TRANSDUCER SETUP

Ongoing work is being carried out on the robotic crawler transducer setup, in previous work a two receiver and bidirectional transmitter was used, bidirectional transmission requires two receivers in order to identify the direction of a reflected wave travelled from, signal direction is essential for ranging and mapping. This setup in the experiment is quite large, Fig. 9, and could easily obstruct crawler movement when moving on top of a real-world subject. As well as this, there are points within a subject that which the waves sent in both directions can return to the two receivers at the same time, this, in turn, makes it impossible to infer the direction of the wave, which means that ranging cannot take place.
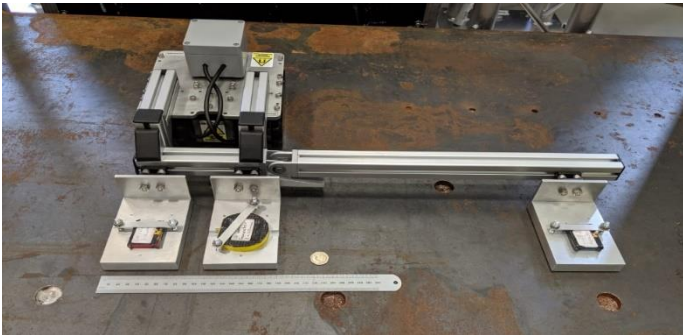

FIGURE 9: PREVIOUSLY USED TWO RECEIVER, BIDIRECTIONAL TRANSMITTER SETUP, APPROXIMATELY 50 CM IN WIDTH.

A solution to this is to use a uni-directional EMAT where waves are generated in only one direction, this removes the need for a second receiver, significantly reducing the width of the transducer setup. This allows the transmitter and receiver to be placed side by side, see Fig. 10, the resultant transducer package will be less than 15cm compared to 50cm. The second receiver can be removed as a uni-directional EMAT that only generates waves in one direction; therefore the propagation path and direction of the wave is always implied, and so the second receiver is not needed to determine signal direction. The use of a unidirectional transmitter EMAT improves robotic crawler mobility and decreases the complexity of signal interpretation.

FIGURE 10: PROTOTYPE UNIDIRECTIONAL TRANSMITTER AND RECEIVER TRANSDUCER SETUP.

7. CONCLUSION

This paper has given an update on the work towards creating an automated guided wave-based mapping robotic crawler system that will be used to create internal maps of large industrial assets. Ongoing work will look to further explore the estimation of defect size and shape, as well as optimising transducer setup for ranging and mapping.

REFERENCES

[1] D. Zonta, B. Glisic, and S. Adriaenssens, 'Value of information: impact of monitoring on decision-making: VALUE OF INFORMATION: IMPACT OF MONITORING ON DECISION-MAKING', *Struct. Control Health Monit.*, vol. 21, no. 7, pp. 1043–1056, Jul. 2014, doi: 10.1002/stc.1631.

[2] J. M. Farley, 'BEST PRACTICE IN THE APPLICATION OF NDT – AN UPDATE', *Mitsui BabcockHSE*, p. 6, 2004.

[3] S. E. Walker and S. Rubin, 'Integrity testing of storage tank structure using robotic ultrasound', US20160299031A1, Oct. 13, 2016 Accessed: May 21, 2020.

[4] C. N. Macleod, G. Dobie, S. G. Pierce, R. Summan, and M. Morozov, 'Machining-Based Coverage Path Planning for Automated Structural Inspection', *IEEE Trans. Autom. Sci. Eng.*, vol. 15, no. 1, pp. 202–213, Jan. 2018, doi: 10.1109/TASE.2016.2601880.

[5] R. Fulbright and L. M. Stephens, 'SWAMI: An autonomous mobile robot for inspection of nuclear waste storage facilities', *Auton. Robots*, vol. 2, no. 3, pp. 225–235, 1995, doi: 10.1007/BF00710858.

[6] A. Kroll, 'A survey on mobile robots for industrial Inspections', Jan. 2008, pp. 406–414. doi: 10.3233/978-1-58603-887-8-406.

[7] S. Soldan, G. Bonow, and A. Kroll, 'RoboGasInspector - A Mobile Robotic System for Remote Leak Sensing and Localization in Large Industrial Environments: Overview and First Results', *IFAC Proc. Vol.*, vol. 45, no. 8, pp. 33–38, 2012, doi: 10.3182/20120531-2-NO-4020.00005.

[8] D. Lattanzi and G. Miller, 'Review of Robotic Infrastructure Inspection Systems', *J. Infrastruct. Syst.*, vol. 23, no. 3, p. 04017004, Sep. 2017, doi: 10.1061/(ASCE)IS.1943-555X.0000353.

[9] C. Mineo, S. G. Pierce, P. I. Nicholson, and I. Cooper, 'Robotic path planning for non-destructive testing – A custom MATLAB toolbox approach', *Robot. Comput.-Integr. Manuf.*, vol. 37, pp. 1–12, Feb. 2016, doi: 10.1016/j.rcim.2015.05.003.

[10] M. Tabatabaeipour, J. Hettler, S. Delrue, and K. V. D. Abeele, 'Visualization of Delaminations in Composite Structures Using a Baseline-Free, Sparse Array Imaging Technique Based on Nonlinear Lamb Wave Propagation', *ACTA Acust. UNITED Acust.*, vol. 103, p. 12, 2017.

[11] M. Tabatabaeipour, J. Hettler, S. Delrue, and K. Van Den Abeele, 'Non-destructive ultrasonic examination of root defects in friction stir welded butt-joints', *NDT E Int.*, vol. 80, pp. 23–34, Jun. 2016, doi: 10.1016/j.ndteint.2016.02.007.

[12] 'Scorpion 2 | Eddyfi'. https://eddyfi.com/en/product/scorpion-2 (accessed Jan. 27, 2020).

[13] 'Novel Solid Contact Ultrasonic Couplants Based on Hydrophilic Polymers'. https://www.ndt.net/article/wcndt00/papers/idn406/idn406.htm (accessed Aug. 15, 2022).

[14] G. Dobie, 'Ultrasonic Sensor Platforms for Non-Destructive Evaluation', p. 308.

[15] 'Solutions', *Hexagon Manufacturing Intelligence*. https://www.hexagonmi.com/en-GB/solutions (accessed Aug. 15, 2022).

[16] H. Durrant-Whyte and T. Bailey, 'Simultaneous localization and mapping: part I', *IEEE Robot. Autom. Mag.*, vol. 13, no. 2, pp. 99–110, Jun. 2006, doi: 10.1109/MRA.2006.1638022.

[17] T. Bailey and H. Durrant-Whyte, 'Simultaneous localization and mapping (SLAM): part II', *IEEE Robot. Autom. Mag.*, vol. 13, no. 3, pp. 108–117, Sep. 2006, doi: 10.1109/MRA.2006.1678144.

[18] M. Tabatabaeipour *et al.*, 'Application of ultrasonic guided waves to robotic occupancy grid mapping', *Mech. Syst. Signal Process.*, vol. 163, p. 108151, Jan. 2022, doi: 10.1016/j.ymssp.2021.108151.

[19] S. Thrun, W. Burgard, and D. Fox, *Probabilistic Robotics*, 1st ed. The MIT Press, 2006.

[20] R. McMillan *et al.*, 'Characterization of EMAT Guided Wave Reflectivity on Welded Structures for use in Ranging', *IEEE Sens. J.*, pp. 1–1, 2022, doi: 10.1109/JSEN.2022.3179326.

[21] A. Huber, 'Dispersion Calculator User's Manual'. Centre for Lightweight Production Technology, Sep. 2021.

[22] M. Tabatabaeipour *et al.*, 'Ultrasonic guided wave estimation of minimum remaining wall thickness using Gaussian process regression', *Mater. Des.*, vol. 221, p. 110990, Sep. 2022, doi: 10.1016/j.matdes.2022.110990.